PAPER • **OPEN ACCESS**

Dynamic response of a floating dock under corrosion-induced accidents

To cite this article: T Zahi *et al* 2023 *IOP Conf. Ser.: Mater. Sci. Eng.* **1294** 012016

Dynamic response of a floating dock under corrosion-induced accidents

T Zahi*, X Wen and M C Ong

Department of Mechanical and Structural Engineering and Materials Science
University of Stavanger, NO-4036, Stavanger, Norway

* Correspondence: 268048@uis.no (Terry Zahi)

Abstract. Dynamic responses of a floating dock under corrosion-induced accidents are studied using a numerical method. The numerical model is proposed to calculate the dynamic responses of the floating dock during operations. It includes a six-degree-of-freedom (6-DOF) model, a hydrostatic force model, a hydrodynamic force model, and a hydraulic model. The effects of the corrosion-induced holes on the stability of the floating dock are investigated and the results show that the maximum pitch and roll angles are 0.18° and 0.69° respectively when there is one hole located at one tank. The maximum pitch and roll angles become 0.42° and 2.04° respectively when there are two holes located at different tanks. The results indicate that situations involving more than one corroded hole result in large roll and pitch angles, which ultimately increase the risk of the vessel capsizing. This analysis not only emphasizes potential hazards but also presents an opportunity for the maritime sector to enhance safety, operational efficiency, and environmental responsibility.

1. Introduction

A floating dock as illustrated in Figure 1 is a specialized pontoon. It plays a crucial role in the maritime industry, serving as essential infrastructure for vessel maintenance, repairs, and cargo handling operations [1]. It is equipped with chambers and has a cross-sectional shape resembling the letter "U." The structure is designed to accommodate varying water levels and provides a stable platform for carrying out these activities. These ballast tanks allow for the adjustment of the floating dock's draft by adding water into them or removing water from them and maintaining the desired trim and heel as the same time [2]. Typically, the process of raising the dock involves pumping out the ballast water, while submerging it is achieved by allowing seawater to flow into the tanks by gravity. The flow rate of the ballast water going into or coming out of each tank is controlled by a valve specifically assigned to that tank. The floating dock is gaining popularity as a solution to address the shortage of dock space in diverse areas of ocean engineering because it eliminates the need for ground yard space [3]. However, they can be subjected to accidental conditions, such as extreme weather events or unexpected equipment failures, which can significantly impact their stability and structural integrity.

Figure 1. Vessel undergoing maintenance on a floating dock [4].

There are two accidents related to the corrosion of the ballast tanks. In one accident, a floating dock sank during a docking operation due to excessive trim caused by the failure of ballast valves following corrosion. This excessive trim submerged the aft vent pipe, leading to rapid flooding of compartments and subsequent sinking of the floating dock at the berth [5]. Another case involved a floating dock sinking due to inaccurate positioning of keel blocks. When the floating dock emerged from the water, several keel blocks punctured the pontoon deck, causing flooding in multiple ballast tanks, rapid loss of buoyancy, and eventual sinking [6].

The aim of this paper is to evaluate the dynamic behaviors of a floating dock under corrosion induced accidents. This evaluation is rendered using a numerical model that has been created to replicate the dynamic operations of the floating dock. This model incorporates several components, including a six-degree-of-freedom (6-DOF) model, a hydrostatic force model, a hydrodynamic force model, and a hydraulic model. The outcomes of this study will provide valuable insights for the maritime industry regarding the maintenance strategies necessary to ensure the safety of floating docks.

2. Numerical model

2.1. Specifications of a floating dock system

Figure 2 shows the floating dock system, where a floating dock, a vessel, mooring ropes connecting the dock and the vessel, mooring lines and the docking blocks on the top deck are shown. The floating dock system is described within a global coordinate system called *OXYZ*. The origin of this coordinate system is positioned at the centre of the dock's keel. The *X*-axis represents the direction along the keel, from the aft side to the fore side. The *Y*-axis is from the starboard to port direction, while the *Z*-axis points vertically upward from the bottom of the dock.

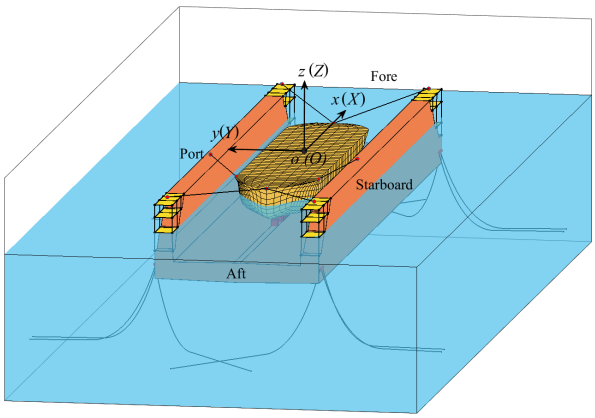

Figure 2. Illustration of a floating dock system.

A body-fixed coordinate system named *oxyz* initially coincide with the global coordinate system. The body-fixed coordinate system moves with the floating dock. It will become different from the global coordinate system as the dock moves. Table 1 shows the specifications of the floating dock system. The Details of the ballast tanks are shown in Figure 3, where the number and the maximum volume of each ballast tank are given.

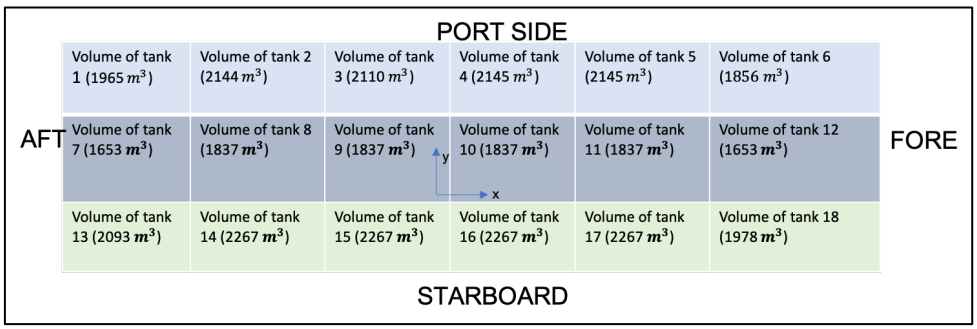

Figure 3. Details of the ballast tanks.

Table 1. Specifications of a floating dock system

Dimension of dock $L_d \times B_d \times H_d$	168.48 m × 39.8 m × 18.2 m
Mass of dock	5.1782×10^6 kg
Initial *X* of the dock's CoG	-0.435 m
Initial *Y* of the dock's CoG	0.093 m
Initial Z of the dock's CoG	5.497 m
Dock's mass moment of inertia $I_{11\text{dock}}$	9.56×10^8 kg · m^2
Dock's mass moment of inertia $I_{22\text{dock}}$	1.026×10^{10} kg · m^2
Dock's mass moment of inertia $I_{33\text{dock}}$	1.096×10^{10} kg · m^2
Dimension of vessel $L_v \times B_v \times H_v$	95.217 m × 20 m × 8 m
Mass of vessel	5.1292×10^6 kg
Initial *X* of the vessel's CoG	-0.435 m
Initial *Y* of the vessel's CoG	0.093 m
Initial *Z* of the vessel's CoG	13.09 m
Vessel's mass moment of inertia $I_{11vessel}$	2.234×10^8 kg · m^2
Vessel's mass moment of inertia $I_{22vessel}$	2.968×10^9 kg · m^2
Vessel's mass moment of inertia $I_{33vessel}$	2.968×10^9 kg · m^2
Density of seawater	1025 kg/m^3
Gravitational acceleration	9.81 m/s^2

2.2. 6-DOF model

The motions of the floating dock are updated using a 6-DOF model. The 6-DOF model includes the dock's translational motion equations in the global coordinate system and the dock's rotational motion equations described in the body-fixed coordinate system. The translational motion equations are given in Eq. (1) based on Newton's Second Law.

$$\frac{\mathrm{d}^2 \boldsymbol{X}_{CG}}{\mathrm{d}t^2} = \boldsymbol{m}^{-1} \sum \boldsymbol{F}_G \tag{1}$$

where $\mathbf{X}_{\mathrm{CG}} = (X_{\mathrm{CG}}, Y_{\mathrm{CG}}, Z_{\mathrm{CG}})$ represents the CoG of the floating dock, $\boldsymbol{m}$ represents the mass matrix of the floating dock. $\boldsymbol{F}_{\mathrm{G}}$ is denoted as the external force vector applied to the CoG. The dock's angular velocity vector is modelled using Eq. (2) [7].

$$\frac{\mathrm{d}\boldsymbol{\omega}_{\mathrm{B}}}{\mathrm{d}t} = \boldsymbol{I}^{-1}\left[\sum \boldsymbol{M}_{\mathrm{B}} - \boldsymbol{\omega}_{\mathrm{B}} \times (\boldsymbol{I}\boldsymbol{\omega}_{\mathrm{B}})\right] \tag{2}$$

where $\boldsymbol{I}$ represents the inertial tensor of the floating dock, $\boldsymbol{M}_{\mathrm{B}}$ is the moment vector and $\boldsymbol{\omega}_{\mathrm{B}} = (\omega_{B1}, \omega_{B2}, \omega_{B3})$ is the dock's angular velocity vector. The rotational angles of the floating dock are computed using Eq. (3)

$$\begin{cases} \dfrac{\mathrm{d}\phi}{\mathrm{d}t} = (\omega_{B2}\sin\gamma + \omega_{B3}\cos\gamma)/\cos\psi \\ \dfrac{\mathrm{d}\psi}{\mathrm{d}t} = (\omega_{B2}\cos\gamma - \omega_{B3}\sin\gamma) \\ \dfrac{\mathrm{d}\gamma}{\mathrm{d}t} = \omega_{B1} + (\omega_{B2}\sin\gamma + \omega_{B3}\cos\gamma)\tan\psi \end{cases} \tag{3}$$

The yaw pitch and roll angles are denoted as ϕ, ψ and γ are the yaw, respectively. The interaction between the dock and the vessel is addressed in an approximate way. The dock and the vessel are considered as a single rigid body with hybrid mass and mass moments of inertia.

2.3. Hydrostatic force model

The buoyancy forces of the dock and vessel, as well as the gravitational forces of water in the ballast tanks are considered as the hydrostatic forces. They are all calculated using the Archimedes' law. To assess the submerged volumes of the floating dock and the ballast tanks, a strip theory is employed, where the three-dimensional (3D) structure is divided into two-dimensional (2D) sections. By integrating the hydrostatic forces along the longitudinal direction of the floating dock and the ballast tanks, the overall hydrostatic loads on the 3D structure are calculated. The submerged regions of the 2D sections are represented by a few boundary points, enabling the determination of their area, first moment of area, and second moment of area. Using the section areas, the displaced water volume of the floating dock, as well as the volume of ballast water, can be computed by the integration along the longitudinal direction.

The height of the water level in a ballast tank is calculated using a secant iteration method of a single point in Eq. (4).

$$h^{(n+1)} = h^{(n)} - \frac{h^{(n)} - h_{\mathrm{pre}}}{V^{(n)} - V_{\mathrm{pre}}}(V^{(n)} - V) \tag{4}$$

In Eq. (4), V is the water volume in a ballast tank, h_{pre} is the water level height in the previous time step and V_{pre} is the water volume in the water level h_{pre}.

2.4. Hydrodynamic force model

The added mass of the floating dock is calculated by forming the 2D results along the longitudinal direction of the dock. The 2D results are based on the added mass and mass moments of inertia of 2D plate. The 3D correction given by the aspect-ratio formula of Pabst [8]. Table 2 shows the results of the floating dock's added mass and mass moments of inertia.

Table 2. Added mass and mass moments of inertia.

Motion	Formula	value
Heave	$\mathrm{m}_{33\mathrm{added}} = \frac{1}{8}\rho\pi\mathrm{B}^2\mathrm{L}\Psi(\mathrm{B/L})$	9.4604×10^7 kg
Roll	$\mathrm{I}_{11\mathrm{added}} = \frac{1}{256}\rho\pi\mathrm{B}^4\mathrm{L}\Psi(\mathrm{B/L})$	4.6830×10^9 kg · m^2
Pitch	$\mathrm{I}_{22\mathrm{added}} = \frac{1}{96}\rho\pi\mathrm{B}^2\mathrm{L}^3\Psi(\mathrm{B/L})$	2.2378×10^{11} kg · m^2

The damping coefficients are modelled based on the mass matrices of the dock, a damping ratio of 5% and natural frequencies of the heave, roll and pitch. According to the DNV recommended practice, when the damping of the system is unknown, a damping ratio of 5% is suggested [9]. The natural frequencies are calculated using Eq. (5) [9].

$$\omega_{\text{heave}} = \sqrt{\frac{C_{33}}{m_{33}}}, \qquad \omega_{\text{roll}} = \sqrt{\frac{C_{44}}{I_{11}}}, \quad \omega_{\text{pitch}} = \sqrt{\frac{C_{55}}{I_{22}}} \tag{5}$$

where m_{33}, I_{11} and I_{22} are the total mass, mass moments of inertia of the floating dock, and C_{33}, C_{44} and C_{55} are the hydrostatic restoring coefficients in heave, roll and pitch motions, respectively.

2.5. Modelling of the ballast water system and the corrosion holes

The ballast system of the floating dock can be divided into six groups and each group can be illustrated in Figure 4. There are six ballast pumps that individually control three ballast tanks positioned from port to starboard, and two types of pipelines with diameters of 400mm and 600 mm. Each ballast tank is equipped with its own butterfly valve, and the main pipes feature inlet and outlet valves used for ballasting and de-ballasting operations, respectively.

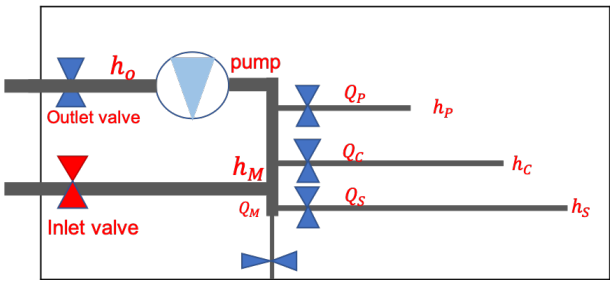

Figure 4. Description of one group of the ballast water system during the de-ballasting operation.

The numerical modelling of the ballast water system is based on the pressure difference characteristics of different elements, i.e., pipe, valve and pump. The difference of water head when the water is passing the element is calculated in Eqs. (6) – (9).

$$h_{\text{O}} - h_{\text{out}} = \lambda_{\text{M}} |Q_{\text{M}}| Q_{\text{M}} \tag{6}$$

$$h_{\text{P}} - h_{\text{M}} = \lambda_{P} |Q_{\text{P}}| Q_{\text{P}} \tag{7}$$

$$h_{\text{C}} - h_{\text{M}} = \lambda_{\text{C}} |Q_{\text{C}}| Q_{\text{C}} \tag{8}$$

$$h_{\text{S}} - h_{\text{M}} = \lambda_{\text{S}} |Q_{\text{S}}| Q_{\text{S}} \tag{9}$$

h_{M}, h_{P}, h_{C}, h_{S}, and h_{o} are the water heads at right sides of pump, port, centre, starboard and outlet (inlet) valves in Figure 4, and h_{out} is the water head at the left side of outlet valve. Q_{M}, Q_{P}, Q_{C} and Q_{S} are the flow rates in main, port, centre and starboard pipes. The coefficients λ_{M}, λ_{P}, λ_{C} and λ_{S} are given by the K_V values of the butterfly valves, as reported by Wen et al. [10].

Table 2. K_V value at different hole diameter for the butterfly valves [10]

Diameter [mm]	40	50	65	80	100	125	150	200	250	300	400
K_V [m³/hour/bar]	53	133	240	410	665	900	1800	3550	7350	9100	10500

The K_V values depend on the diameter of the corrosion hole and are given by experimental measurements [11]. λ can be written as Eq. (10).

$$\lambda = \frac{1}{\text{g}(\text{KV}/36000)^2} \quad [\text{s}^2/\text{m}^5] \tag{10}$$

The water head difference when the water is passing through pumps is calculated using Eq. (11).

$$h_{\text{O}} - h_{\text{M}} = h_0 - \lambda_{\text{pump}} |Q_{\text{M}}| Q_{\text{M}} \tag{11}$$

where $h_0 = 21.25$ m is the pump's total water head when $Q_M = 0$, and $\lambda_{\text{pump}} = 20\ \text{s}^2/\text{m}^5$ is the pump coefficient. A continuity equation between the main pipe and the branch pipes is modelled in Eq. (12).

$$Q_{\mathrm{M}} = Q_{\mathrm{P}} + Q_{\mathrm{C}} + Q_{\mathrm{S}} \tag{12}$$

For the ballasting operation, the solution is given by taking $h_0 = 0$ and $\lambda_{\mathrm{pump}} = 0$. The flow rate through the hole is then given by Eq. (13)

$$Q = \frac{(h_{out} - h)}{\sqrt{\lambda_{hole}|h_{out} - h|}} \tag{13}$$

Where λ_{hole} is hole coefficient. After the flow rate of a ballast tanks is obtained, the ballast water volume is updated using Eq. (14).

$$\frac{\mathrm{d}\alpha_j}{\mathrm{d}t} = \frac{Q_j}{V_{\mathrm{max},j}} \tag{14}$$

where α_j is the volume fraction of the water in j^{th} ballast tank, $V_{\mathrm{max},j}$ is the total volume of j^{th} tank and Q_j is the corresponding flow rate.

3. Results and discussions

3.1. Case description

The maximum pitch and roll angles of the floating dock are investigated. The dock is initially docking a vessel on top without heel and trim at the draught of 3.5m. The dock will tilt when there is corrosion hole located at one of two ballast tanks. This present study involves two scenarios: one is that a corrosion-induced hole with different diameters occurs in one single ballast tank during the ballasting operation and another is that two ballast tanks have corrosion-induced holes of 300mm each.

The sensitivity study of section number for the dock and the ballast tanks, and the convergence study of the water levels in ballast tanks were conducted by Zhang et al. [12]. According to the convergent results of these sensitivity studies, the dock's section number is chosen as 150 and the section number of each ballast tank is selected as 20 in the present study. In a dock's section, 18 points are used while those of port, centre and starboard tanks are 8, 8 and 6, respectively.

3.2. Dynamic behaviours

To guarantee the dock's performance under these unexpected circumstances, a time-step sensitivity analysis is to be conducted. Figure 5 shows the time-step sensitivity study of the draught, pitch and roll angles during the corrosion induced accident in Tank No.1, where the hole diameter is 50mm. Three time-steps of 1s, 0.5 s, and 0.25 s are examined to assess the convergence of the results. The results obtained using these three different time steps appeared the almost same, a time step of 0.5s is chosen to proceed the further analysis to achieve a balance between the computational time and the temporal resolution. As can be seen in Figure 6, the draught becomes larger as the weight of the ballast water increases. The dock continues to tilt with final heel and trim angles of 0.55° and 0.14° respectively.

Figure 6 shows the roll and pitch angles for the scenarios of one corrosion hole with different diameters located at Tank. No.01. The roll and pitch angles of different hole diameters have the same final convergent results. Table 5 presents the time taken to fill up the ballast tank through the corrosion hole in Tank No. 01. The time is recorded when the flow rate through the hole decreases to $0.5 \times 10^{-3}\ \mathrm{m}^3/\mathrm{s}$. From the table, the time increases with a decreasing hole diameter. For a hole diameter of 300mm, the dock tilts to the maximum heel and trim in about half an hour.

Table 3. Time taken to fill up the ballast tank through the corrosion hole in Tank No. 01.

Hole diameter [mm]	Duration time [hour]
50.00	21.34
100.00	4.39
150.00	1.63
200.00	0.83
250.00	0.40
300.00	0.32

Figure 7 shows the maximum pitch and roll angle for the scenarios of one corrosion hole with a diameter of 300mm located at different ballast tanks. A large maximum pitch angle corresponds to the hole located at the tanks near the aft or fore, and a large maximum roll angle corresponds to the hole located at the tanks near the port or starboard. It can be attributed to the moment due to the extra weight of the ballast water flow into the tank through the corrosion hole. The maximum roll angles of the scenarios of one corrosion hole located at the starboard tanks are always larger than those at the port tanks. The reason is that the total volumes of the starboard tanks are larger than those of the port tanks, as shown in Figure 3. Figure 8 shows the volumes of the ballast water in Tanks No.02 and 014 for the scenarios of one corrosion hole located at Tanks No.02 and 014, respectively. The volume of the ballast water in Tank No. 14 is much larger than that in Tank No.02, which can also explain the reason of the different maximum roll angle in Figure 6(b).

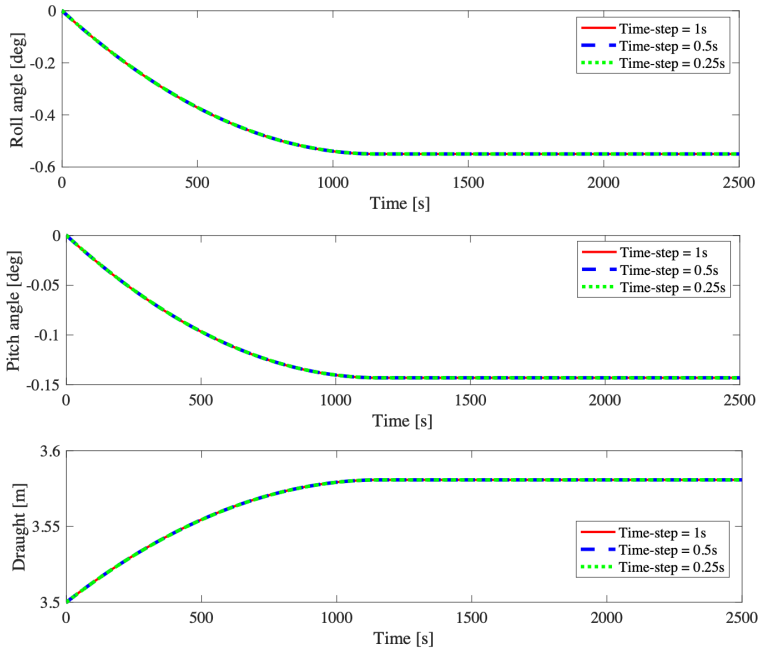

Figure 5. Time-step sensitivity study of the roll, pitch angles and draught during the corrosion induced accident in Tank No. 01, where the hole diameter is 50 mm.

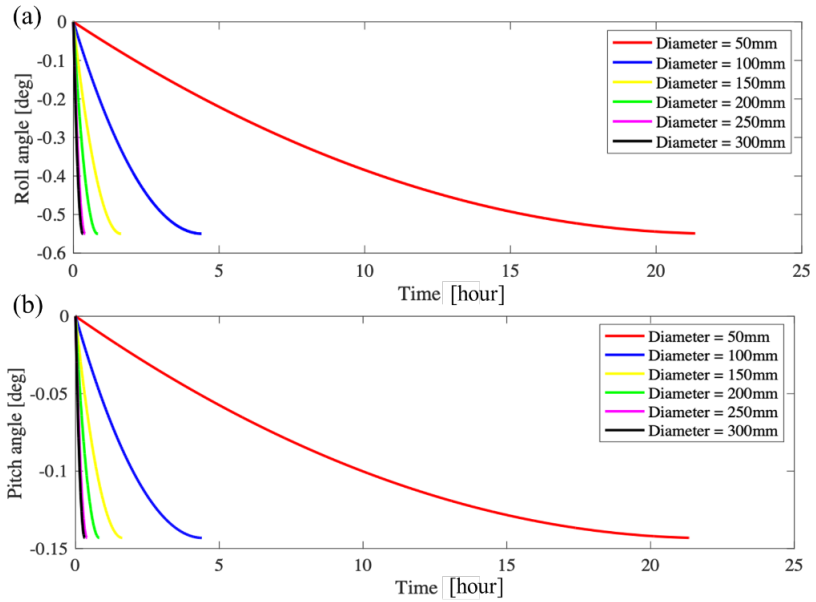

Figure 6. Roll and pitch angles for the scenarios of one corrosion hole with different diameters located at Tank. No.01.

0.14	0.09	0.03	0.03	0.09	0.14
0.17	0.11	0.03	0.03	0.11	0.17
0.18	0.12	0.04	0.04	0.11	0.17

(a) Maximum pitch angle [°]

0.55	0.58	0.54	0.56	0.58	0.55
0.00	0.00	0.00	0.00	0.00	0.00
0.72	0.75	0.71	0.68	0.71	0.69

(b) Maximum roll angle [°]

Figure 7. Maximum pitch and roll angles for the scenarios of one corrosion hole with a diameter of 300 mm located at different ballast tanks.

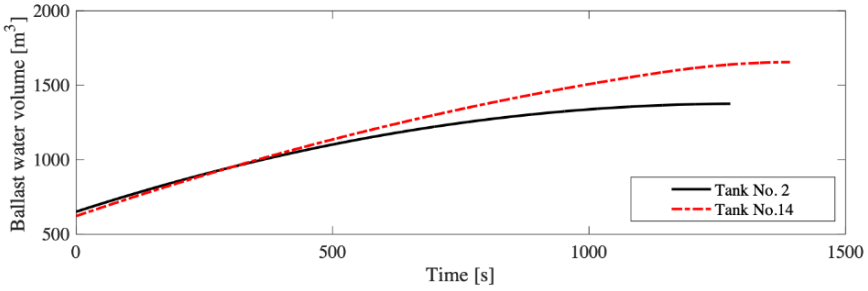

Figure 8. Volumes of the ballast water in Tanks No.02 and 014 for the scenarios of one corrosion hole located at Tanks No.02 and 014, respectively.

Figures 9 and 10 shows the maximum pitch angles for the scenarios of two corrosion holes with a diameter of 300 mm located at different ballast tanks. The distributions follow the principle as discussed for one corrosion hole cases. A large maximum pitch angle corresponds to the holes located at the tanks near the aft or fore, and a large maximum roll angle corresponds to the holes located at the tanks near the port or starboard. The maximum pitch and roll angles for two corrosion hole cases are 0.42° and 2.04° respectively.

tank No.	1	2	3	4	5	6	7	8	9	10	11	12	13	14	15	16	17	18
1	0.14	0.30	0.21	0.13	0.06	0.00	0.35	0.27	0.19	0.12	0.05	0.00	0.31	0.24	0.17	0.11	0.05	0.00
2	0.30	0.09	0.15	0.07	0.00	0.06	0.29	0.21	0.14	0.06	0.00	0.06	0.25	0.19	0.12	0.06	0.00	0.05
3	0.21	0.15	0.03	0.00	0.06	0.12	0.18	0.13	0.06	0.00	0.06	0.11	0.17	0.11	0.06	0.00	0.05	0.10
4	0.13	0.07	0.00	0.03	0.14	0.21	0.12	0.06	0.00	0.06	0.13	0.19	0.11	0.06	0.00	0.06	0.11	0.17
5	0.06	0.00	0.06	0.14	0.09	0.32	0.06	0.00	0.06	0.13	0.21	0.28	0.05	0.00	0.06	0.12	0.19	0.25
6	0.00	0.06	0.12	0.21	0.32	0.14	0.00	0.05	0.12	0.19	0.27	0.35	0.00	0.05	0.11	0.17	0.24	0.31
7	0.35	0.29	0.18	0.12	0.06	0.00	0.17	0.32	0.22	0.14	0.06	0.00	0.42	0.32	0.22	0.13	0.06	0.00
8	0.27	0.21	0.13	0.06	0.00	0.05	0.32	0.11	0.16	0.07	0.00	0.06	0.33	0.24	0.15	0.07	0.00	0.06
9	0.19	0.14	0.06	0.00	0.06	0.12	0.22	0.16	0.03	0.00	0.07	0.13	0.22	0.15	0.07	0.00	0.07	0.13
10	0.12	0.06	0.00	0.06	0.13	0.19	0.14	0.07	0.00	0.03	0.15	0.22	0.13	0.07	0.00	0.07	0.15	0.22
11	0.05	0.00	0.06	0.13	0.21	0.27	0.06	0.00	0.07	0.15	0.11	0.33	0.06	0.00	0.07	0.16	0.24	0.33
12	0.00	0.06	0.11	0.19	0.28	0.35	0.00	0.06	0.13	0.22	0.33	0.17	0.00	0.06	0.14	0.22	0.32	0.42
13	0.31	0.25	0.17	0.11	0.05	0.00	0.42	0.33	0.22	0.13	0.06	0.00	0.18	0.39	0.27	0.16	0.07	0.00
14	0.24	0.19	0.11	0.06	0.00	0.05	0.32	0.24	0.15	0.07	0.00	0.06	0.39	0.12	0.19	0.09	0.00	0.08
15	0.17	0.12	0.06	0.00	0.06	0.11	0.22	0.15	0.07	0.00	0.07	0.14	0.27	0.19	0.04	0.00	0.09	0.16
16	0.11	0.06	0.00	0.06	0.12	0.17	0.13	0.07	0.00	0.07	0.16	0.22	0.16	0.09	0.00	0.04	0.18	0.26
17	0.05	0.00	0.05	0.11	0.19	0.24	0.06	0.00	0.07	0.15	0.24	0.32	0.07	0.00	0.09	0.18	0.11	0.41
18	0.00	0.05	0.10	0.17	0.25	0.31	0.00	0.06	0.13	0.22	0.33	0.42	0.00	0.08	0.16	0.26	0.41	0.17

Figure 9. Maximum pitch angles (°) for the scenarios of two corrosion holes with a diameter of 300 mm located at different ballast tanks.

tank No.	1	2	3	4	5	6	7	8	9	10	11	12	13	14	15	16	17	18
1	0.55	1.44	1.34	1.26	1.18	1.12	0.68	0.64	0.60	0.57	0.54	0.51	0.02	0.02	0.02	0.01	0.01	0.01
2	1.44	0.58	1.41	1.36	1.31	1.26	0.69	0.66	0.63	0.61	0.59	0.57	0.02	0.01	0.01	0.01	0.01	0.01
3	1.34	1.41	0.54	1.26	1.24	1.22	0.59	0.58	0.57	0.56	0.56	0.55	0.02	0.02	0.02	0.02	0.02	0.02
4	1.26	1.36	1.26	0.56	1.34	1.35	0.58	0.58	0.59	0.59	0.60	0.61	0.01	0.01	0.01	0.01	0.02	0.02
5	1.18	1.31	1.24	1.34	0.58	1.54	0.57	0.59	0.61	0.63	0.66	0.68	0.01	0.01	0.02	0.02	0.02	0.02
6	1.12	1.26	1.22	1.35	1.54	0.55	0.51	0.54	0.56	0.60	0.64	0.67	0.01	0.02	0.02	0.02	0.02	0.02
7	0.68	0.69	0.59	0.58	0.57	0.51	0.00	0.00	0.00	0.00	0.00	0.00	0.83	0.78	0.73	0.68	0.64	0.61
8	0.64	0.66	0.58	0.58	0.59	0.54	0.00	0.00	0.00	0.00	0.00	0.00	0.81	0.78	0.75	0.72	0.69	0.67
9	0.60	0.63	0.57	0.59	0.61	0.56	0.00	0.00	0.00	0.00	0.00	0.00	0.72	0.71	0.70	0.69	0.68	0.67
10	0.57	0.61	0.56	0.59	0.63	0.60	0.00	0.00	0.00	0.00	0.00	0.00	0.67	0.68	0.69	0.70	0.71	0.72
11	0.54	0.59	0.56	0.60	0.66	0.64	0.00	0.00	0.00	0.00	0.00	0.00	0.67	0.69	0.72	0.75	0.78	0.81
12	0.51	0.57	0.55	0.61	0.68	0.67	0.00	0.00	0.00	0.00	0.00	0.00	0.61	0.65	0.68	0.73	0.78	0.84
13	0.02	0.02	0.02	0.01	0.01	0.01	0.83	0.81	0.72	0.67	0.67	0.61	0.72	1.90	1.79	1.67	1.56	1.47
14	0.02	0.01	0.02	0.01	0.01	0.02	0.78	0.78	0.71	0.68	0.69	0.65	1.90	0.75	1.87	1.78	1.71	1.64
15	0.02	0.01	0.02	0.01	0.02	0.02	0.73	0.75	0.70	0.69	0.72	0.68	1.79	1.87	0.71	1.71	1.68	1.66
16	0.01	0.01	0.02	0.01	0.02	0.02	0.68	0.72	0.69	0.70	0.75	0.73	1.67	1.78	1.71	0.68	1.68	1.71
17	0.01	0.01	0.02	0.02	0.02	0.02	0.64	0.69	0.68	0.71	0.78	0.78	1.56	1.71	1.68	1.68	0.71	2.04
18	0.01	0.01	0.02	0.02	0.02	0.02	0.61	0.67	0.67	0.72	0.81	0.84	1.47	1.64	1.66	1.71	2.04	0.69

Figure 10. Maximum roll angles (°) for the scenarios of two corrosion holes with a diameter of 300 mm located at different ballast tanks.

4. Conclusion

The dynamic responses of a floating dock under corrosion-induced accidents are studied using a numerical method. The numerical model is proposed to calculate the dynamic responses of the floating dock during operations. It includes a six-degree-of-freedom (6-DOF) model, a hydrostatic force model, a hydrodynamic force model, and a hydraulic model. The effects of the corrosion-induced holes on the stability of the floating dock are investigated and the results show that the maximum pitch and roll angles are 0.18° and 0.69° respectively when there is one hole located at one tank. The maximum pitch and roll angles become 0.42° and 2.04° respectively when there are two holes located at different tanks. The results indicate that situations involving more than one corroded hole result in larger roll and pitch angles, which ultimately increase the risk of the vessel capsizing. This analysis not only emphasizes potential hazards but also presents an opportunity for the maritime sector to enhance safety, operational efficiency, and environmental responsibility.

References

[1] Wankhede A, 2021, Dry Dock, Types of Dry Docks & Requirements for Dry Dock, last modified 9 January 2021. https://www.marineinsight.com/guidelines/dry-dock-types-of-dry-docks-requirements-for-dry-dock/#Types_of_Dry_Dock. Accessed 14 March 2023.

[2] Yoon K, Kim H-J, Yeo S, Hong Y, Cha J and Chung H 2020 Ballasting plan optimization for operation of a 2D floating dry dock, *Structural Engineering and Mechanics.* 74(4), 521–532.

[3] Shan X, Yu Q, Tian J 2009 Risk management of mooring operation of floating dock," Journal of Tianjin University Science and Technology. Technol. **42**, 335-339.

[4] ASRY (2023) Arab ship building and repair yard company, available at: https://www.asry.net (accessed Sep. 01, 2023)

[5] Morra T 2011 The Evolutionary Development of Floating Dry Docks, Master's Thesis, East Carolina University, East Carolina.

[6] El-Maadawy M, Moustafa M M, El-Kilani H S and Tawfiq A A 2018 Structural safety assessment of a floating dock during docking operation, Port-said Engineering Research Journal. **22**(2), 32 - 39.

[7] Schaub H and Junkins J L 2003 Analytical Mechanics of Space Systems. American Institute of Aeronautics and Astronautics (AIAA), Inc., Reston, VA, pp. 23,77-123.

[8] Pabst W 1930 Theory of the landing impact of seaplanes,NTRS – NASA Technical Report. Available at: https://ntrs.nasa.gov/api/citations/19930094836/downloads/19930094836.pdf.

[9] Det Norske Vertias (DNV) (2012), DNV Recommended Practice DNV-RP-C205:Environmental conditions and environmental loads.

[10] Wen X, García Conde A, Zhang J, and Ong M C 2023 Numerical modelling of a floating dock and its automatic control, in Proceedings of the 42nd International Conference on Offshore Mechanics and Arctic Engineering. American Society of Mechanical Engineers, Melbourne, Australia, June 11–16, 2023. (Submitted: OMAE2023-102873).

[11] Eurotorc, Butterfly valve engineering data, Nov. 12, 2022. https://www.eurotorc.com/butterfly-valve-engineering-data.html. (accessed Sep. 16, 2023).

[12] Zhang J, Wen X, Ong M C 2023 Development of a Floating Dock Numerical Model and the Ballast Water Distribution Strategy. Proc. ASME 2023 42nd Int. Conf. Ocean, Offshore and Arctic Eng. **5**: Ocean Eng.. Melbourne, Australia. June 11–16, 2023. V005T06A068. ASME. https://doi.org/10.1115/OMAE2023-102996